ON THE ANGULAR RESOLUTION OF THE *AGILE* GAMMA-RAY IMAGING DETECTOR

S. Sabatini[1,2], I. Donnarumma[1,2], M. Tavani[1,2,3], A. Trois[4], A. Bulgarelli[5], A. Argan[1], G. Barbiellini[6], P. W. Cattaneo[7],
A. Chen[8], E. Del Monte[1], V. Fioretti[5], F. Gianotti[5], A. Giuliani[9], F. Longo[6], F. Lucarelli[10], A. Morselli[2,3],
C. Pittori[10], F. Verrecchia[10], AND P. Caraveo[9]

[1] INAF/IAPS-Roma, I-00133 Roma, Italy
[2] INFN Roma Tor Vergata, I-00133 Roma, Italy
[3] Dip. di Fisica, Univ. Tor Vergata, I-00133 Roma, Italy
[4] INAF-OAC, I-09012 Capoterra, Italy
[5] INAF/IASF-Bologna, I-40129 Bologna, Italy
[6] Dipartimento di Fisica and INFN Trieste, I-34127 Trieste, Italy
[7] INFN-Pavia, I-27100 Pavia, Italy
[8] School of Physics, 1 Jan Smits Av., Braamfontein 2000 Johannesburg, SouthAfrica
[9] INAF/IASF-Milano, I-20133 Milano, Italy
[10] ASI Science Data Center, I-00044 Frascati, Roma, Italy

ABSTRACT

We present a study of the angular resolution of the *AGILE* gamma-ray imaging detector (GRID) that has been operational in space since 2007 April. The *AGILE* instrument is made of an array of 12 planes that are each equipped with a tungsten converter and silicon microstrip detectors, and is sensitive in the energy range 50 MeV–10 GeV. Among the space instruments devoted to gamma-ray astrophysics, *AGILE* uniquely exploit an analog readout system with dedicated electronics coupled with silicon detectors. We show the results of Monte Carlo simulations carried out to reproduce the gamma-ray detection by the GRID and we compare them to in-flight data. We use the Crab (pulsar + Nebula) system for discussion of real data performance, since its E^{-2} energy spectrum is representative of the majority of gamma-ray sources. For Crab-like spectrum sources, the GRID angular resolution (FWHM of ∼4° at 100 MeV; ∼0°.8 at 1 GeV; ∼0°.9 integrating the full energy band from 100 MeV to tens of GeV) is stable across a large field of view, characterized by a flat response up to 30° off-axis. A comparison of the angular resolution obtained by the two operational gamma-ray instruments, *AGILE*/GRID and *Fermi*/LAT (Large Area Telescope), is interesting in view of future gamma-ray missions, which are currently under study. The two instruments exploit different detector configurations that affect the angular resolution: the former is optimized in the readout and track reconstruction, especially in the low-energy band, the latter is optimized in terms of converter thickness and power consumption. We show that despite these differences, the angular resolution of both instruments is very similar, between 100 MeV and a few GeV.

Key words: gamma rays: general – instrumentation: detectors – methods: data analysis

1. INTRODUCTION

Gamma-ray astrophysics in space have enormously advanced since the first detection of photons above 100 MeV (Kraushaar et al. 1972). The progression of space missions and instruments over the past decades (*OSO*-3, SAS-2, COS-B, Energetic Gamma-ray Experiment Telescope; EGRET, on board the *Compton Gamma-ray Observatory; CGRO*) has led to improvements of the overall detector performance, in terms of both angular resolution and sensitivity. In addition to this, the progressively wider field of view (FoV) has allowed a continuous monitoring of the variable gamma-ray sky. Following early cosmic gamma-ray detection by the *OSO*-3 satellite (Kraushaar et al. 1972), the first gamma-ray telescope, SAS-2, launched in 1972, reached an angular resolution of a few degrees (Fichtel et al. 1975). This mission was followed by the European mission COS-B, launched in 1975 August 8, and operational for seven years (Mayer-Hasselwander et al. 1979; Swanenburg et al. 1981). The *CGRO*, active between 1991 and 2000, provided the first complete investigation of the gamma-ray sky. In particular, *CGRO* hosted the EGRET, operating in the energy range 30 MeV–30 GeV (Thompson et al. 1993; Fichtel & Trombka 1997; Thompson 1998). Pre-*AGILE*/Pre-*Fermi* space instruments were mostly based on spark chamber technology.

Further improvements to the overall performance of gamma-ray detectors in space became possible with the advent of solid-state silicon detector technology. The scientific objectives of the new generation of instruments required the following enhancements: (1) improving the gamma-ray angular resolution near 100 MeV by at least a factor of 2–3 compared to EGRET; (2) obtaining the largest possible FoV at 100 MeV, reaching 2.5–3 sr; and (3) increasing flux sensitivity near 100 MeV. The current generation of gamma-ray space instruments, *AGILE*/GRID (Gamma-ray Imaging Detector) and *Fermi*/LAT (Large Area Telescope), launched in 2007 April and 2008 June, respectively, were designed to achieve these objectives. Both instruments make use of tungsten–silicon detectors for the conversion and detection of gamma-ray photons, with a common overlapping energy range in the ∼50 MeV–10 GeV band (Atwood & the Fermi LAT Collaboration 2009; Tavani et al. 2009). The gamma-ray detector is structured to form a "Silicon Tracker" made of several trays, each containing a tungsten layer (used as a converter of the incident γ-ray photon into an e^+/e^- pair) and two silicon strip layers (used to track the the e^+/e^- pair path across the instrument through their (x, y) projections along each tray). The detected tracks are identified and fitted by a Kalman filter that allows for the reconstruction of the original direction and

energy of the incident photon. The main source of contamination in the detection of γ-ray photons is then by charged particle tracks, which can be confused with e^+/e^- pairs. For this reason, background rejection filters are used both on board and on-ground, to process the data and obtain a final discrimination and classification of the events.

An important parameter in the assessment of the overall instrument scientific performance is the resulting angular resolution, i.e., the minimum distance at which two close sources are distinguished as separated. The point-spread function (PSF) describes the response of an imaging instrument to a point source and the angular resolution is usually described by either the FWHM of the PSF radial profile or the 68% containment radius ($CR_{68\%}$) of the PSF. Key parameters of the instrument configuration affecting the angular resolution of γ-ray solid-state silicon detectors are:

1. the size of the silicon strips (the pitch) and the silicon detector readout system (e.g., either digital or analog), resulting in a different effective spatial resolution of the particle trajectory due to charge coupling between adjacent silicon strips;
2. the distance between consecutive silicon planes that, combined with the spatial resolution, defines the limiting angular resolution;
3. the thickness of tungsten layers promoting gamma-ray photon conversion, and at the same time inducing multiple scattering that leads to a degradation of the charged particle tracks; and
4. the reconstruction and event classification algorithms.

Table 4 in the appendix summarizes the main characteristics of the *AGILE* and *Fermi* gamma-ray detectors, whose configurations are different in several ways: the former is optimized in the readout and track reconstruction, especially in the low-energy band, and the latter is optimized in terms of converter thickness, geometrical area, and power consumption. An important difference between the two instruments, which can be crucial for the scientific performance of the instrument, is the readout system (analog for the *AGILE/*GRID and digital for *Fermi/*LAT).

In the following sections, we focus on the characterization of the *AGILE/*GRID angular resolution both from simulations and from in-flight data. In Section 2 we define the parameters that are used across the paper to describe the instrument angular resolution; Section 3 describes the Monte Carlo (MC) simulation setup and data processing pipeline; Section 4 shows the results from the MC simulations; Section 5 compares the results of the simulation with the in-flight data angular resolution. This paper complements the work by Chen et al. (2013): here we focus on simulations characterizing the overall performance of the GRID instrument, and in a special study of Crab-like sources, the simulations that reproduce the behavior of the majority of detected cosmic gamma-ray sources; we also present a direct comparison of *AGILE* and *Fermi* in-flight data for the Crab,[1] and discuss the results concerning the angular resolution in terms of the different instrument configurations (Section 6), which can be crucial in the study of future missions.

---

[1] The case of the Vela pulsar has been addressed by Chen et al. (2013) and (Ackermann et al. 2013).

2. THE ANGULAR RESOLUTION

For an imaging telescope, the response in terms of the reconstructed positions of a set of photons from a point-like source in the sky defines its PSF. Since this function can be considered azimuthally symmetric in γ-ray telescopes for incidence angles within $30°$ as used in this paper, the effect of the dispersion can be described as a function of one parameter: the angular distance α between reconstructed and nominal direction. Defining the PSF radial profile, $P(\alpha)$, as the probability distribution per steradian of measuring an incoming photon at a given angular distance α from its true direction, we therefore have

$$\mathrm{PSF}(\alpha)d\alpha = 2\pi \sin(\alpha)P(\alpha)d\alpha.$$

In the following, we adopt two parameters that are widely used in the literature to assess the angular resolution in terms of the "width" of the PSF (e.g., Thompson et al. 1993):

1. the FWHM of the probability distribution per steradian, $P(\alpha)$; and
2. the $CR_{68\%}$ of the probability distribution, $\mathrm{PSF}(\alpha)$.

The $CR_{68\%}$ is strongly related to the source image compactness; since it takes into account the whole contribution of the source profile and is more affected by possible extended tails. In contrast, the FWHM is mainly determined by the central core emission of the source.

3. SETUP AND DATA PROCESSING OF THE *AGILE* SIMULATED DATA

In order to fully understand how the instrument configuration and the data analysis pipeline affect the final angular resolution of a gamma-ray telescope, we carried out dedicated MC simulations of the *AGILE*/GRID, analyzing simulated data with the same pipeline used to process in-flight data. The simulations were carried out using an available simulation tool ("GAMS," GEANT *AGILE* MC Simulator; Cocco et al. 2002; Longo et al. 2002), implemented during the development phase of the *AGILE* mission. The tool makes use of the GEANT3 environment[2] and takes into account all the main components of the *AGILE* instrument configuration: the spacecraft (bus) *MITA* and the *AGILE* payload, consisting of the CsI Mini-calorimeter, the silicon–tungsten Tracker, the Anticoincidence system, the X-ray detector (Super-*AGILE*), the thermal shield, the mechanical structure, and the lateral electronics boards. The tool allows us to simulate a parallel front of a given direction for both charged particles and/or photons and their interactions across the instruments. The spectral energy distribution of the front can be monochromatic or with any given law. The simulated tracks are then processed by the DHSIM, the Data Handling SIMulator (Argan 2004; Argan et al. 2008), which implements the onboard algorithms for a first track reconstruction, event classification, and background rejection (Giuliani et al. 2006). The DHSIM output is a data file in the same format as the AGILE in-flight telemetry and can be processed using the same pipeline as that used for real data analysis. Further background rejection techniques are applied to the data on-ground, producing the final classification of the events. The currently used filter for the scientific analysis of the *AGILE/*GRID data ("FM3.119") was also used in this paper for the processing of the simulated data.

---

[2] http://wwwasd.web.cern.ch/wwwasd/geant/index.html

Table 1
Results from the Simulations of Monochromatic Photon Parallel Beams

		AGILE/GRID PSF HWHM				
Centroid Energy (MeV)	Energy Band (MeV)	$\theta = 1°$ $\phi = 0°$ (deg)	$\theta = 1°$ $\phi = 45°$ (deg)	$\theta = 30°$ $\phi = 0°$ (deg)	$\theta = 30°$ $\phi = 45°$ (deg)	Err (deg)
50	30–70	4.0	4.5	4.5	4.5	0.5
100	70–140	2.25	2.25	2.5	2.25	0.25
200	140–300	1.1	1.2	1.3	1.2	0.1
400	300–700	0.7	0.7	0.7	0.7	0.1
1000	700–1700	0.4	0.4	0.4	0.4	0.1
5000	1700–10000	0.2	0.2	0.2	0.2	0.1

Note. Half-width at half-maximum of the PSF radial profile in degrees. Events for the different energy channels are selected on the basis of the reconstructed energy; this is the same selection process that is used for real data.

Table 2
Results from the Simulations of Monochromatic Photon Parallel Beams

		AGILE/GRID PSF $CR_{68\%}$				
Centroid Energy (MeV)	Energy Band (MeV)	$\theta = 1°$ $\phi = 0°$ (deg)	$\theta = 1°$ $\phi = 45°$ (deg)	$\theta = 30°$ $\phi = 0°$ (deg)	$\theta = 30°$ $\phi = 45°$ (deg)	Err (deg)
50	30–70	7.5	7.5	8.5	8.5	0.5
100	70–140	4.3	4.3	4.7	5.0	0.25
200	140–300	2.2	2.2	2.6	2.7	0.1
400	300–700	1.2	1.2	1.3	1.4	0.1
1000	700–1700	0.6	0.6	0.6	0.7	0.1
5000	1700–10000	0.3	0.3	0.3	0.3	0.1

Note. 68% Containment radius of the PSF in degrees. Events for the different energy channels are selected on the basis of the reconstructed energy; this is the same selection process that is used for real data.

Each simulation contains 2×10^5 photons that cross the tracker and the data are analyzed with the same pipeline as for real data. Typical efficiency after background rejection within 30° off-axis angle is ~30%, leaving therefore a set of ~5×10^4 events classified as photons and used for our calculations in the paper.

4. THE ANGULAR RESOLUTION FOR SIMULATED AGILE/GRID DATA

With the aim of investigating the dependence of the telescope angular resolution upon the energy of incoming photons and their incident direction in the FoV, we carried out simulations of parallel fronts of photons by varying those parameters.

We describe the incident direction as the composition of a zenith angle θ (i.e., the angular distance of the incoming photon direction from the vertical axis of the Tracker, also named the off-axis angle) and an azimuthal angle φ (i.e., the angular distance between a given axis in the instrument plane and the projection of the incoming direction in the plane). Since the detector response is mostly azimuthally symmetric, we expect the main dependence to be upon θ. Simulations were carried out for the following values of these angles: $\theta = (1°, 30°, 50°)$

[3]; $\phi = (0°, 45°)$. Two different sets of simulations were performed:

1. parallel fronts of monochromatic photons of energies 50, 100, 200, 400, 1000, 5000 MeV; and
2. parallel fronts of photons with a Crab-like photon spectrum of the type $E^{-2.1}$, in the energy range 30 MeV–50 GeV.

The simulated data are analyzed with the same pipeline as that used for the real data. In particular, data were analyzed using the most recent pipeline for the data processing ("BUILD21") and instrument response functions ("I0023").
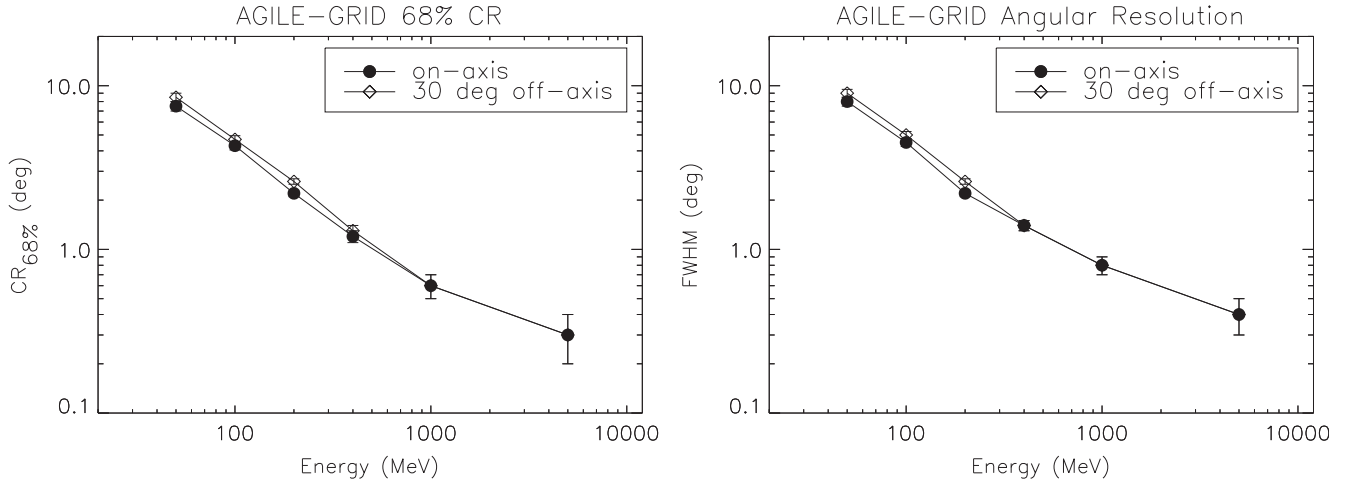
4.1. Monochromatic Photons

Monochromatic simulated data can be used for an ideal characterization of the instrument response and were simulated for different energies and different incident directions as previously described.

According to the definitions given in Section 2, Tables 1 and 2 and Figure 1 show the values obtained for the half-width at half-maximum (HWHM)[4] (calculated from the PSF radial profile) and for the $CR_{68\%}$ (calculated from the PSF) for different energies and different off-axis angles. We use both

---

[3] For the on-axis case we use a value of $\theta = 1°$, since the case of $\theta = 0°$ induces a singularity in the software that generates the parallel front of photons. For our purposes $\theta = 1°$ resembles the on-axis case.

[4] Here we show the HWHM instead of the FWHM used in the figures in order to help with a direct comparison with the $CR_{68\%}$ and in the identification of the width of the radial profile (see, e.g., Figure 2, right panel).

Figure 1. Left panel: *AGILE/*GRID 68% containment radius vs. photon energy for simulated monochromatic photons of different incident angles. Right panel: angular resolution (FWHM) vs. photon energy, shown for comparison to the CR68.
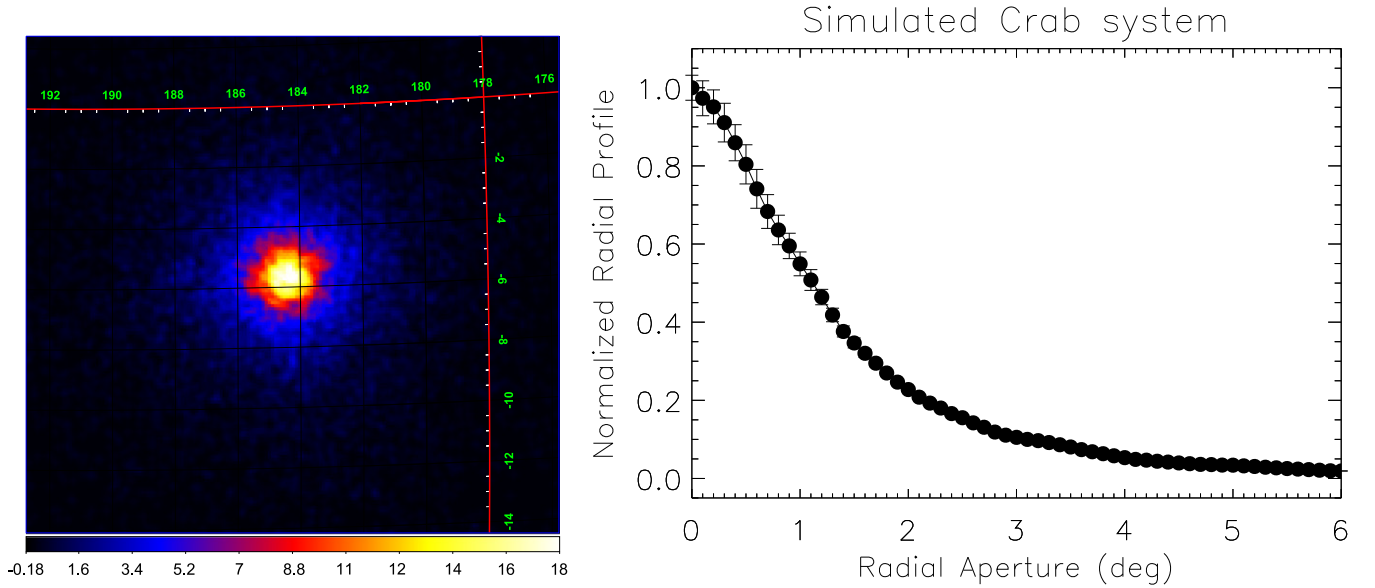
Figure 2. Left panel: count map of the simulated Crab system in the 100–400 MeV energy band. Pixel size is $0°.1$. Right panel: average count radial profile. The counts are normalized to the maximum value of the profile in order to reach 1 at 0°. The error bars are the Poissonian values.

parameters for simplifying the comparison with previous papers, related both to gamma rays or to other wavelengths. In the rest of the paper we prefer adopting the FWHM to describe the angular resolution of the instruments in order to be more compliant with the definition in the multi-frequency domain.

Note that for this analysis we do not fit the PSF with any specific function, we just obtain the above parameters from the raw distribution of the reconstructed directions (see, e.g., Figure 2, right panel). The source radial profile is given by the average source counts within circular crowns of increasing radii, centered at the source centroid. The instrumental background counts are subtracted by evaluating their contribution in a circular crown at distances large enough to avoid contamination by the source tails (see, e.g., Figure 5). In Tables 1 and 2 we also report the intrinsic error in the estimate, given by the bin size of the profile, which has a minimum value
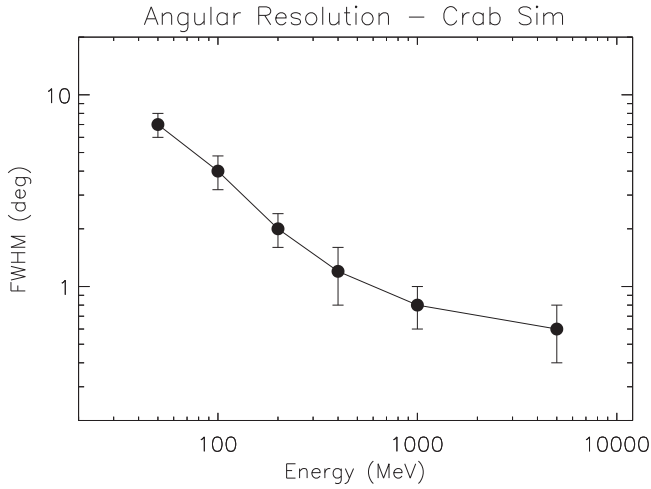
of $0°.1$. This value is the minimum bin size allowed for the generation of typical count maps in the *AGILE* real data for high significance sources. At the same time this value allowed us to have a statistical significance well above the 5σ per bin in the radial profiles that is used to calculate the FWHM with the adopted number of simulated input events.

Table 1 shows that the *AGILE* angular resolution, as inferred from the FWHM, is stable across the instrument's FoV up to 30° of the off-axis angle. Table 2 shows that on the contrary, the $CR_{68\%}$ increases slightly with off-axis angle below 1000 MeV, since this parameter is much more affected by tails in the radial profile than the FWHM. This is expected, since at 30° off-axis angle tracks pass through much more material compared to the on-axis case: this causes a higher dispersion in the reconstructed direction due to the effect of multiple scatterings, which are more pronounced below 1000 MeV (see Section 6).

Table 3
HWHM of the *AGILE*/GRID PSF Radial Profile for Different Energy Channels and Off-axis Angles for the Crab Simulations

				HWHM for the Crab Simulations				
Centroid Energy (MeV)	Energy Band (MeV)	$\theta = 1°$ $\phi = 0°$ (deg)	$\theta = 1°$ $\phi = 45°$ (deg)	$\theta = 30°$ $\phi = 0°$ (deg)	$\theta = 30°$ $\phi = 45°$ (deg)	$\theta = 50°$ $\phi = 0°$ (deg)	$\theta = 50°$ $\phi = 45°$ (deg)	Err (deg)
50	30–70	3.5	3.5	3.0	3.0	3.0	4.0	0.5
100	70–140	2.0	2.0	2.0	2.0	2.4	2.4	0.4
200	140–300	1.0	1.2	1.2	1.2	1.4	1.4	0.2
400	300–700	0.6	0.6	0.8	0.8	0.8	0.8	0.2
1000	700–1700	0.4	0.4	0.4	0.4	0.4	0.4	0.1
5000	1700–10000	0.3	0.3	0.3	0.3	0.3	0.3	0.1
100–400	100–400	0.9	0.9	0.9	1.0	1.1	1.0	0.1
400–1000	400–1000	0.45	0.45	0.35	0.35	0.45	0.35	0.1
100–50000	100–50000	0.50	0.50	0.40	0.40	0.45	0.30	0.1

Figure 3. *AGILE*/GRID angular resolution vs. photon energy for the simulation of an on-axis Crab-like source.

4.2. Simulations of Crab-like Sources

Simulations of Crab-like spectrum sources were carried out as previously described and as an example, Figure 2 shows a count map obtained from the MC simulated data for the 100–400 MeV energy band at the (30°, 0°) incident direction (left panel) and the average radial profile of the source (right panel). The map was obtained by the simulated event list using the same pipeline as that for producing real data maps.

Table 3 shows the results of the whole analysis for the Crab simulations at varying photon energy and incident direction. The instrument response is stable within 30° across the FoV within the errors, and the overall response is dominated by the zenith angle (θ), since the dependency upon the azimuthal angle is minimal, if any. Figure 3 shows the angular resolution as a function of photon energy for on-axis incident directions.

We also report in Table 3 the HWHM for the typical broadbands used in the *AGILE*/GRID data analysis, i.e., the 100–400 MeV, the 400–1000 MeV channels, and the 100 MeV–50 GeV full band, which gives on average an angular resolution of $1°\!.8 \pm 0°\!.2$, $0°\!.8 \pm 0°\!.2$, and $0°\!.9 \pm 0°\!.2$ for off-axis angles within 30°, respectively. These values will be compared to the ones obtained with the in-flight data analysis.

It is interesting to compare the results of the Crab simulations to the monochromatic photon beams (see Tables 3 and 1): the values of the angular resolution per energy channels agree within the errors, showing that the contribution of possible energy channel cross talk is negligible.

5. IN-FLIGHT DATA ANALYSIS

The whole simulation setup and the above results for the angular resolution can be validated by a comparison with the values obtained by in-flight data. The *AGILE* satellite has been operational since 2007 July and the angular resolution of the GRID has been studied both on-ground (Cattaneo et al. 2012; Cattaneo & Rappoldi 2013) and in-flight (Chen et al. 2013). Here, however, we focus in particular on the case of the Crab source (pulsar + Nebula) whose spectral energy distribution in the gamma-ray energy band is dominated by the pulsar and is described by a power law with a spectral index of ∼2.1. As previously mentioned, this spectral energy distribution is representative of the majority of the gamma-ray sources and we therefore think that it is an ideal test case to assess the instrument response, also in view of future gamma-ray missions under study (see the next section). We selected *AGILE* data from a long-term pointing of the region (11 days, 2007-09-23T12:01:05–2007-10-04T12:01:05) during which the source was located at an off-axis angle ⩽30°. Due to the resulting overall exposure of the region, hereafter we focus on two wide energy bands in order to obtain a good photon statistics for a robust assessment of the angular resolution: the 100–400 MeV and 400 MeV–1 GeV energy bands. Figures 4 and 5 show the Crab intensity map for the two energy bands, respectively, and the average count radial profile for the source. The FWHM associated with these profiles turns out to be $2°\!.5 \pm 0°\!.5$ in the 100–400 MeV energy range and $1°\!.2 \pm 0°\!.5$ for the 400 MeV–1 GeV band. The good agreement with the results from the simulations (see Table 3) validates the whole setup and data analysis carried out for the simulations.

6. *AGILE* AND *FERMI*: COMPARISON OF IN-FLIGHT DATA FOR THE CRAB SYSTEM

As already mentioned in Section 1, despite implementing the same silicon–tungsten detector concept, the instrument configurations for the *AGILE*/GRID and *Fermi*/LAT detectors are quite different in terms of converter thickness, distance between trays, and spacing between adjacent silicon strips
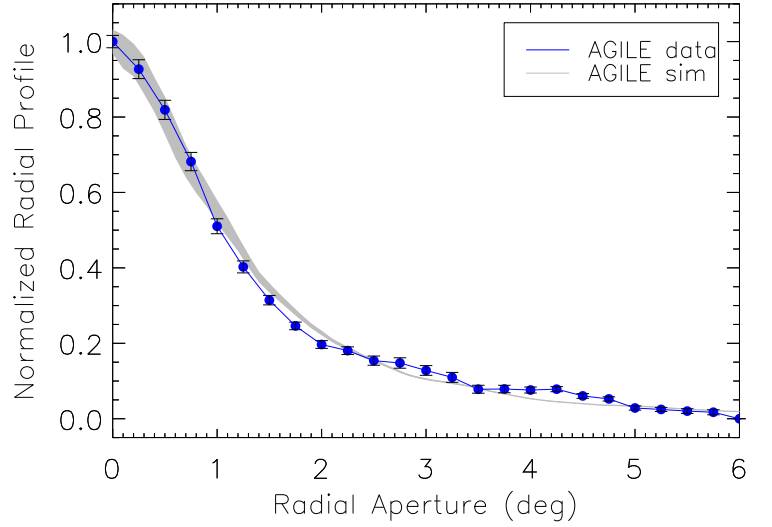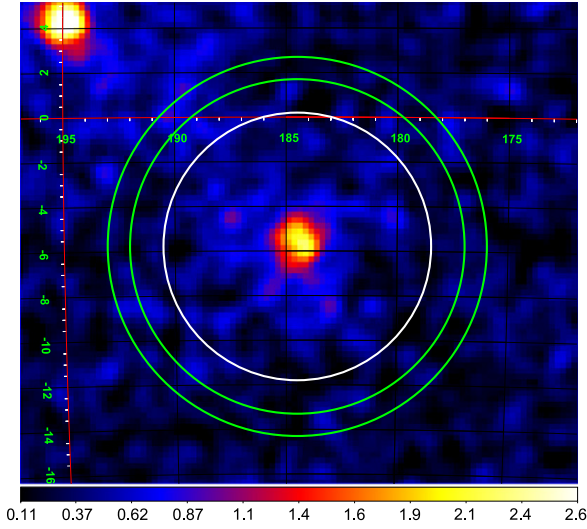
Figure 4. Left panel: *AGILE/*GRID count map of the Crab system (pulsar + Nebula) for the period 2007-09-23T12:01:05-2007-10-04T12:01:05 in the 100–400 MeV energy band; the white circle shows the maximum aperture (6°) used to produce the radial profile of the source shown in the right panel; green circles show the crown region used to estimate the background emission (7°.5–8°.5 radius). Right panel: average count radial profile: blue data points are the in-flight data, while the gray shaded region shows the profile for the simulated crab system with errors. The counts are normalized to the maximum value of the profile in order to reach 1 at 0°. The source in the upper left corner is Geminga.
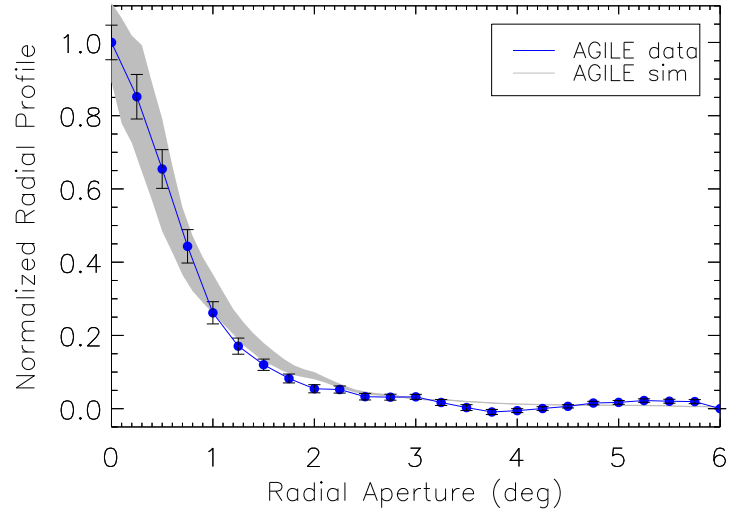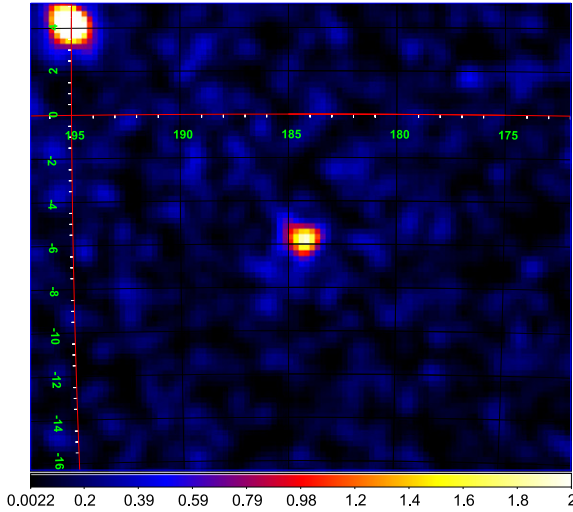

Figure 5. Left panel: *AGILE/*GRID count map of the Crab system (pulsar + Nebula) in the 400–1000 MeV energy band. Right panel: average count radial profile: blue data points are in-flight data, while the gray shaded region shows the profile of the simulated crab system with errors. The counts are normalized to the maximum value of the profile in order to reach 1 at 0°.

(see Table 4). In the case of the *AGILE/*GRID, the silicon tracker is composed of 10 tungsten converter planes of homogeneous thickness (0.07 radiation length each), plus two additional planes without a converter (for a total of 12 planes); the overall GRID radiation length is ∼1$X_\circ$ (Barbiellini et al. 2002; Prest et al. 2003). The *Fermi/*LAT has 12 tungsten planes of ∼0.03 radiation length thickness ("LAT-front") and an additional set of four tungsten planes of 0.18 radiation length ("LAT-back"), plus two planes without a converter (Atwood & the Fermi LAT Collaboration 2009). In both instruments, each tungsten plane is interleaved with two layers of silicon strip detectors that are sensitive to charged particles and are used for the *x*, *y* positioning of the e⁺/e⁻ pair track resulting from the pair conversion. The ratio of strip pitch to

vertical spacing between tracker planes is 0.007 for both *Fermi/*LAT and *AGILE/*GRID.

An important difference between the two instruments is the silicon tracker readout system, which is analog for *AGILE/*GRID and digital for *Fermi/*LAT. Barbiellini et al. (2002) and Prest et al. (2003) extensively describe the GRID's dedicated front-end electronics, characterizing the effective spatial resolution for particle incidence between 0° and 30° and comparing the performances of digital and analog readouts. Although the *GRID* analog readout is structured to read only odd-numbered strips with no signal pickup at even-numbered strips ("floating strip readout"), the capacitive coupling between adjacent strips allows us to obtain a complete sampling of the particle hit positions, discriminating between
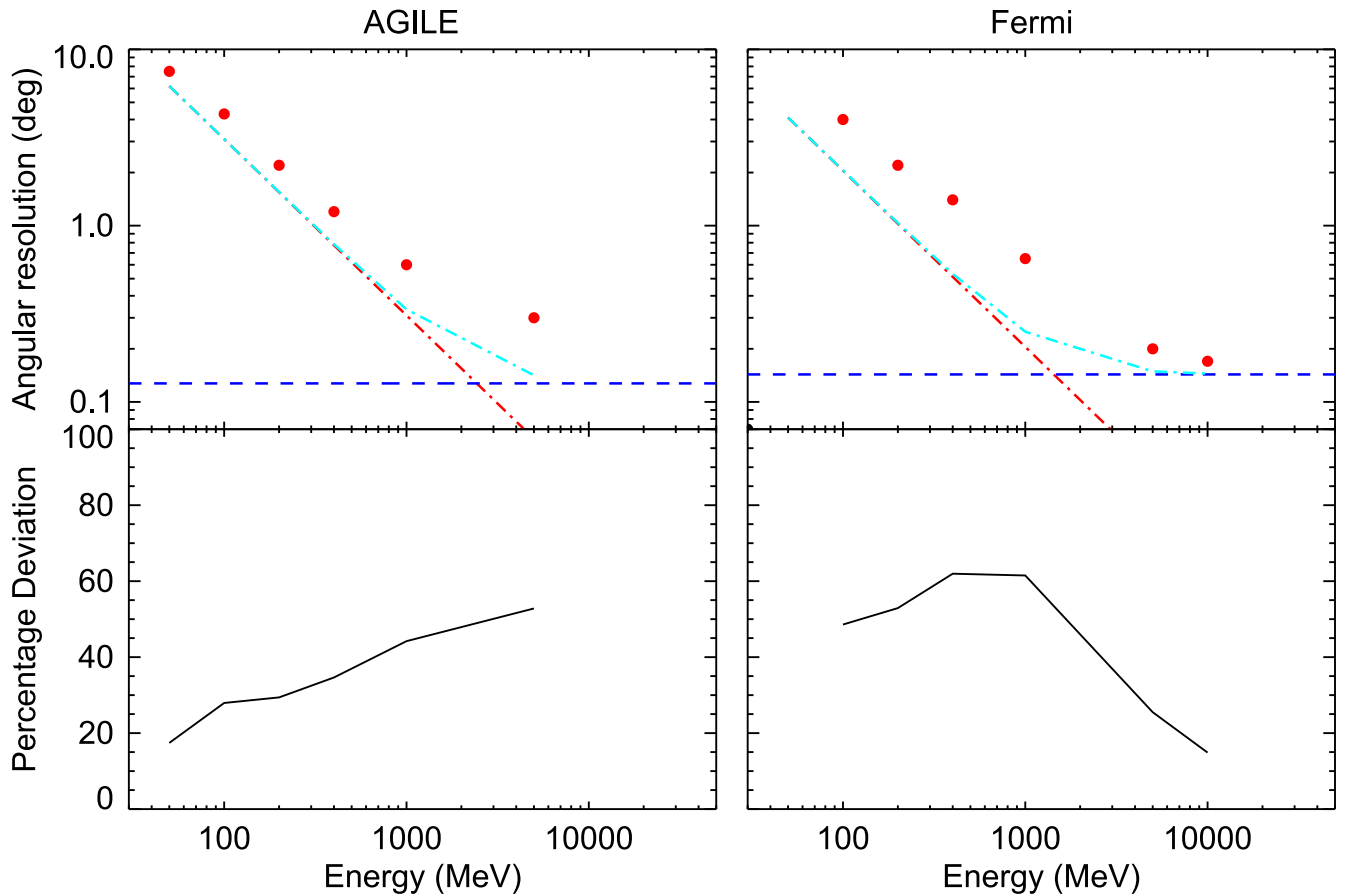
Figure 6. Comparison of the expected limiting values for the angular resolution (dot–dashed cyan line) to the measured ones (red points). Left panel: *AGILE*/GRID simulated Crab data. Right panel: *Fermi*/LAT PSF68 (http://www.slac.stanford.edu/exp/glast/groups/canda/lat_Performance.htm). Top panels: the overall limiting angular resolution is plotted in cyan and is obtained by the combination of: (1) the ratio of the spatial resolution to the distance of consecutive trays (dashed blue line); and (2) the multiple scattering limit (red dot–dashed line). Bottom panels: percentage deviation of the measured angular resolution from the overall expected limiting value.

hits involving directly read and unread microstrips. Typically, each particle hit is characterized by a signal spread out over several adjacent readout-strips (a "cluster"). GRID events produce energy deposition histograms per cluster, which are very well characterized and typically result in 2–3 triggered strips depending on off-axis angle (Fedel et al. 2000; Barbiellini et al. 2002). Note that also for on-axis incidence, a cluster is composed of a minimum of two strips. The effective spatial resolution obtained by the GRID for particle incidence between 0° and 30° is $\delta_s \sim 40\ \mu$m, substantially less than the silicon microstrip size of 121 μm (see Figure 15 in Barbiellini et al. 2002). The advantage of the analog versus the digital readout for the resulting spatial resolution of silicon strip detectors is discussed in Barbiellini et al. 2002 for the *AGILE* tracker configuration, showing an improvement of a factor of 2 (i.e., $\delta_s \sim 40\ \mu$m versus $\delta_s \sim 80\ \mu$m).

The *Fermi*/LAT system is based on a digital readout. The LAT Tracker is non-homogeneous and is characterized by two different values for the angular resolution, one for the "LAT-front" and the other for the "LAT-back" (Ackermann et al. 2013). In the following, we only use LAT-front data for comparison with the *AGILE*/GRID, proving the best angular resolution for *Fermi*. Also note that *Fermi* usually operates in scanning mode, with sources observed most of the time at large off-axis angles, with a consequent degradation of

the angular resolution for a given source, compared to the on-axis performance.

In order to compare the angular resolution of the two instruments at similar conditions, we selected *Fermi* data of the Crab system in pointing mode. We therefore analyzed a comparable set of data, with an exposure ensuring similar photon statistics and with both gamma-ray detectors in pointing mode. The *AGILE* data in pointing mode[5] that was used for this comparison are the data described in Section 5. The *Fermi* data consist of 4 days of integration in the period 2012-07-04T23:24:44–2012-07-08T10:44:43 during which the satellite was stably pointing at the Crab following a gamma-ray flaring episode, with the source located at 10° of the off-axis angle in the FoV. We used the best available quality cut for the *Fermi* data, (the"ULTRA-CLEAN" event class, LAT-front photons, P7REP) in order to optimize the angular resolution of the data. We focus on the analysis of two representative energy bands for *AGILE* in order to have robust statistics for both instruments: 100–400 MeV and 400–1000 MeV.

Figure 7 shows the intensity maps for the two gamma-ray telescopes in the two energy bands and Figure 8 shows the corresponding radial profiles. The resulting angular resolution deduced from the in-flight data are the same, even though the

---

[5] An analysis of *AGILE*/GRID data in "spinning mode" will be discussed in a forthcoming paper by F. Lucarelli et al. (2015, in preparation).
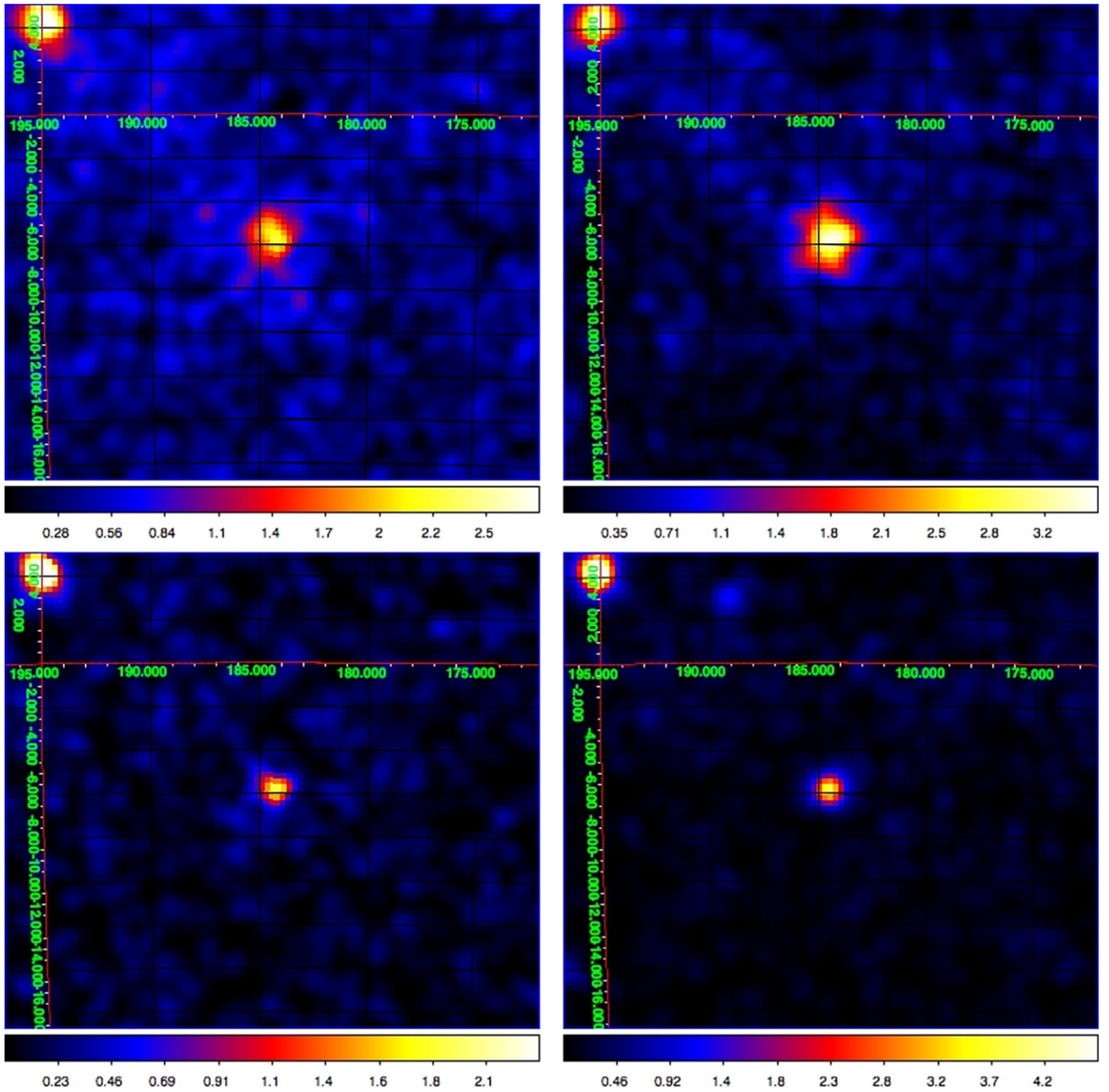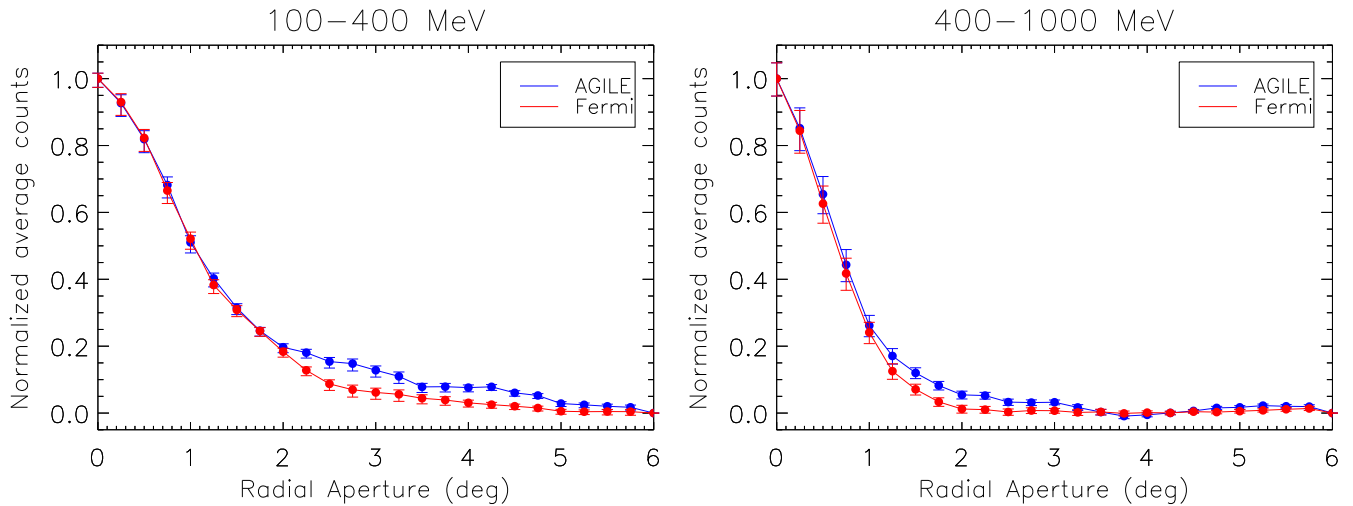
Figure 7. *AGILE/*GRID (left panels) and *Fermi/*LAT (right panels) in-flight count maps for the Crab region in the 100–400 MeV and 400–1000 MeV energy bands, respectively. The pixel size is $0.°25$. Note that the color intensity scale is set so that each map has the maximum value of the scale corresponding to the Crab peak counts.

AGILE data show a more pronounced non-Gaussian tail, due to the converter thickness: the FWHM is $2.°5 \pm 0.°5$ and $1.°2 \pm 0.°5$ in the energy ranges 100–400 MeV and 400 MeV–1 GeV, respectively.

As already mentioned, several factors determine the instrument angular resolution as a function of gamma-ray photon energy, including: (1) multiple scattering; (2) the effective spatial resolution; (3) the photon energy reconstruction; (4) specific particle track reconstruction algorithms; and (5) quality cuts. Figure 6 shows the relative contribution of these factors as a function of energy for both trackers, *AGILE* and *Fermi*. Regarding the multiple scattering, we assume an effective radiation length per tray of 0.085 and 0.04 for *AGILE/*

GRID and *Fermi/*LAT, respectively, taking into account the contributions of the tungsten converter and the supporting material.[6] The top panels show that the multiple scattering effect dominates the overall angular resolution up to 700 MeV and 350 MeV for the two instruments. The bottom panels show the percentage deviation of the measured angular resolution to the overall expected limiting value. The amplitude of the deviation quantifies the reconstruction accuracy, which is

---

[6] In the case of *AGILE* the effective radiation length due to the supporting material for each tray is $\sim 0.015 X_\circ$ from laboratory measurements; since *Fermi* has a similar tray structure (Atwood & the Fermi LAT Collaboration 2009) we assume a similar contribution of $\sim 0.01 X_\circ$.

Figure 8. Average count radial profiles for circular apertures of increasing radii at steps of $0°\!.25$ of the Crab (pulsar + Nebula); in-flight data for the *AGILE/*GRID (blue data points) and *Fermi/*LAT (red data points). Left panel: 100–400 MeV energy range. Right panel: 400–1000 MeV energy range.

optimized in different energy ranges for the two instruments: the accuracy is below 40% up to 400 MeV in the case of *AGILE* and above 2 GeV in the case of *Fermi*. Besides the different tracker configuration, crucial features distinguishing the two instruments and affecting the final reconstruction accuracy are the effective spatial resolution and the quality of the reconstruction algorithms.[7] Therefore we believe that in view of future gamma-ray missions (e.g., Galper et al. 2013; Morselli et al. 2013) the optimization of the angular resolution should not only rely on a reduced converter thickness, but also on the implementation of an analog readout system if the power budget allows it, together with an optimization of the reconstruction algorithms.

7. CONCLUSIONS

The current generation of gamma-ray space instruments is based on silicon detector technology and associated electronics. Both *AGILE/*GRID and *Fermi/*LAT show a quite stable performance in orbit, which is the basis for prolonged operations (*AGILE* is in its 9th year of life in space and *Fermi* is in its 8th year). Compared to the previous generation, the instrument performance improvements both in terms of sensitivity and angular resolution are well established.

In this paper, we summarized the main results concerning the GRID angular resolution, a crucial feature of the *AGILE* instrument, on the basis of the scientific performance of a gamma-ray detector together with its FoV and background rejection capabilities at energies below 400 MeV, allowing for the best exploitation of the instrument configuration. We showed that the *AGILE/*GRID angular resolution is optimized given the overall characteristics of the detector and allows for state-of-the-art mapping of Galactic and extragalactic regions/ sources: the FWHM for off-axis angles in the range of 0°–30° is ∼4° at 100 MeV, and ∼0°.8 at 1 GeV. The angular resolution is quite uniform in the FoV up to 30° off-axis. The FWHM obtained from in-flight data in pointing mode is 2°.5, in the range of 100–400 MeV, and ∼1°.2 in the 400 MeV–1 GeV.

Although the *AGILE/*GRID multiple scattering due to the heavy converter is relatively high, we have proved that a crucial role is played by the optimization of the readout system (analog) of the silicon tracker and of the particle track reconstruction algorithms.[8]

The GRID angular resolution as a function of gamma-ray energies is shown in Figure 1 as resulting from simulations. These values are in good agreement with those deduced from in-flight data as demonstrated in this paper for Crab-like sources.

Furthermore, by a direct comparison of in-flight data of the Crab system, we find that despite the differences in structure, geometry, readout system, and overall size, the *AGILE/*GRID and *Fermi/*LAT-front show similar angular resolutions at energies between 100 MeV and 1 GeV, due to different optimizations of the readout systems and reconstruction algorithms.

APPENDIX
THE *AGILE*/GRID VERSUS *FERMI*/LAT

AGILE is an ASI Small Scientific Mission (Tavani et al. 2009) with a total weight of 320 kg. It carries a scientific instrument dedicated to high-energy astrophysics whose heart is the GRID. Complementary items are the imaging Super-

---

[7] Note that ongoing developments for the track reconstruction algorithms and event classifications for both *AGILE* (updated FM filter) and *Fermi/*LAT (PASS8) may lead to further improvements of the current angular resolution.

[8] It is interesting to note that the *AGILE* Tracker configuration is quite similar to the basic element of the gamma-ray instrument currently under study for the GAMMA-400 mission (Galper et al. 2013). The analog readout of a silicon tracker with *AGILE*-like characteristics is required to optimize the angular resolution with a thick converter (which in the case of GAMMA-400 is currently designed to be ∼0.08 $X_\circ$ per plane).

Table 4
A Comparison Between the *AGILE*/GRID and *Fermi*/LAT

Parameter	*AGILE*/GRID	*Fermi*/LAT
Number of towers	1	16
Total number of Tracker planes	12	18
Vertical spacing (s) between adjacent planes	1.8 cm	3.2 cm
Silicon tile size	9.5×9.5 cm^2	8.95×8.95 cm^2
Silicon detector array for each plane	4×4	4×4
Silicon-strip pitch (δ_P)	121 μm	228 μm
Readout pitch	242 μm	228 μm
Signal readout	analog	digital
Ratio δ_P/s	0.007	0.007
Tungsten converter thickness per plane	0.07 X_o	0.03 X_o (front)
		0.18 (back)
Number of planes with W converter	10	12 (front)
		4 (back)
On-axis total radiation length	0.9	0.5 (front)
		0.8 (back)
Total n. of readout channels	36,864	884,736
Power consumption/channels	400 μW	180 μW

AGILE detector, which is sensitive in the range 20–60 keV (Feroci et al. 2007), the Mini-calorimeter (Labanti et al. 2006), and the Anticoincidence system (Perotti et al. 2006). *AGILE* was launched in 2007 April and is operational in an equatorial orbit of an average height of 530 km.

Fermi is a NASA mission of a large class with a broad international Collaboration. Its imaging gamma-ray instrument is based on a 16-unit Tracker (LAT; Atwood & the Fermi LAT Collaboration 2009), which is complemented by a massive Calorimeter and an Anticoincidence system. *Fermi* was launched in 2008 June in an orbit with inclination of 25° and an average height of 550–600 km.

Table 4 summarizes the main parameters of the two instrument configurations, which are relevant for the angular resolution determination.

REFERENCES

Ackermann, M., Ajello, M., Allafort, A., et al. 2013, ApJ, 769, 54
Argan, A., et al. 2004, in Proc. IEEE-NSS, 1, 371
Argan, A., Tavani, M., Trois, A., et al. 2008, in NSS IEEE (IEEE), 774
Atwood, W. B. & the Fermi LAT Collaboration 2009, ApJ, 697, 1070
Barbiellini, G., Fedel, G., Liello, F., et al. 2002, NIMPA, 490, 146
Cattaneo, P. W., Argan, A., Boffelli, A., et al. 2012, NIMPA, 674, 55
Cattaneo, P. W., & Rappoldi, P. 2013, NIMPB, 239, 241
Chen, A., Argan, A., Bulgarelli, A., et al. 2013, A&A, 558, 37
Cocco, V., Longo, F., & Tavani, M. 2002, NIMPA, 486, 623
Fedel, G., Barbiellini, G., Liello, F., et al. 2000, Proc. SPIE, 4140, 274
Feroci, M., Costa, E., Soffitta, P., et al. 2007, NIMPA, 581, 728
Fichtel, C. E., Hartman, R. C., Kniffen, D. A., et al. 1975, ApJ, 198, 163
Fichtel, C. E., & Trombka, J. I. 1997, Gamma-Ray Astrophysics, Vol. 1386 (NASA Reference Publication)
Galper, A. M., et al. 2013, in Proc. Int. Cosmic-Ray Conf. arXiv:1306.6175
Giuliani, A. 2003, The Kalman Algorithm for the AGILE Mission, PhD thesis, Univ. Milan
Giuliani, A., Cocco, V., Mereghetti, S., Pittori, C., & Tavani, M. 2006, NIMPA, 568, 692
Hartman, R. C., Bertsch, D. L., Bloom, S. D., et al. 1999, ApJS, 123, 79
Kraushaar, W. L., Clark, G. W., Garmire, G. P., et al. 1972, ApJ, 177, 341
Labanti, C., Marisaldi, M., Fuschino, F., et al. 2006, Proc. SPIE, 6266, 62663
Longo, F., Cocco, V., & Tavani, M. 2002, NIMPA, 486, 610
Mayer-Hasselwander, H. A., Kanbach, G., Sieber, W., et al. 1979, ICRC, 1, 206
Morselli, A., Argan, A., Barbiellini, G., et al. 2013, NuPhS, 239, 193
Perotti, F., Fiorini, M., Incorvaia, S., Mattaini, E., & Sant'Ambrogio, E. 2006, NIMPA, 556, 228
Prest, M., Barbiellini, G., Bordignon, G., et al. 2003, NIMPA, 501, 280
Swanenburg, B. N., Bennett, K., Bignami, G. F., et al. 1981, ApJ, 243, 69
Tavani, M., Barbiellini, G., Argan, A., et al. 2009, A&A, 502, 995
Thompson, D. J., Bertsch, D. L., Fichtel, C. E., et al. 1993, ApJS, 86, 629
Thompson, D. J., et al. 1998, Proc. 4th CGRO Symp., AIP Conf. Ser., 410, 39
Yang, H. J., Roe, B. P., & Zhu, J. 2005, NIMPA, 555, 370